

Over-the-Air Federated Learning in MIMO Cloud-RAN Systems

Haoming Ma, Xiaojun Yuan, *Senior Member, IEEE*, Zhi Ding, *Fellow, IEEE*,

Abstract

To address the limitations of traditional over-the-air federated learning (OA-FL) such as limited server coverage and low resource utilization, we propose an OA-FL in MIMO cloud radio access network (MIMO Cloud-RAN) framework, where edge devices upload (or download) model parameters to the cloud server (CS) through access points (APs). Specifically, in every training round, there are three stages: edge aggregation; global aggregation; and model updating and broadcasting. To better utilize the correlation among APs, called inter-AP correlation, we propose modeling the global aggregation stage as a lossy distributed source coding (L-DSC) problem to make analysis from the perspective of rate-distortion theory. We further analyze the performance of the proposed OA-FL in MIMO Cloud-RAN framework. Based on the analysis, we formulate a communication-learning optimization problem to improve the system performance by considering the inter-AP correlation. To solve this problem, we develop an algorithm by using alternating optimization (AO) and majorization-minimization (MM), which effectively improves the FL learning performance. Furthermore, we propose a practical design that demonstrates the utilization of inter-AP correlation. The numerical results show that the proposed practical design effectively leverages inter-AP correlation, and outperforms other baseline schemes.

Index Terms

Federated learning, cloud radio access network, multiple-input multiple-output multiple access channel, lossy distributed source coding, over-the-air computation.

H. Ma and X. Yuan are with the National Key Laboratory of Science and Technology on Communication, the University of Electronic Science and Technology of China, Chengdu, China (e-mail:hmma@std.uestc.edu.cn; xjyuan@uestc.edu.cn). Z. Ding is with the Department of Electrical and Computer Engineering, University of California at Davis, Davis, CA 95616 USA (e-mail:zding@ucdavis.edu). The corresponding author is Xiaojun Yuan.

I. INTRODUCTION

With the growing amount of data stored on mobile edge devices, there is an increasing interest in providing artificial intelligence (AI) services, such as computer vision [1] and natural language processing [2], at the wireless edge. Traditional machine learning (ML) methods require uploading local data to a central node for model training, which unfortunately incurs significant communication costs and raises concerns about data privacy. To address these issues, federated learning (FL) has emerged as a promising framework for distributed and confidential model training [3]. In the FL framework, each edge device trains its local model using its local data and sends its model update to a cloud server (CS) (referred to as uplink transmission). The CS aggregates the local model updates and updates the global model parameters, and then broadcasts the updated global model to the edge devices (referred to as downlink transmission). Compared to centralized learning, FL significantly reduces the communication burden and the risk of data breaches, and therefore becomes a compelling option for machine learning applications at the wireless edge.

The FL uplink involves transmitting a massive amount of model updates from distributed edge devices to the CS, which poses a critical communication bottleneck due to limited uplink channel resources, such as bandwidth, time, and space [4]. Over-the-air computation has been adopted to improve the communication efficiency of the FL uplink by supporting analog model uploading from massive edge devices [5]. Unlike orthogonal resource allocation among devices to avoid interference, over-the-air FL (OA-FL) enables devices to share radio resources during model uploading by leveraging the signal-superposition property of analog transmission for model aggregation over the air. Pioneering work has confirmed that OA-FL has strong noise tolerance [6] and can reduce latency substantially compared with the FL schemes based on conventional orthogonal multiple access (OMA) protocols. The authors in [7] have further extended over-the-air FL to the multiple input multiple output (MIMO) channel, and leveraged the beamforming technology to enhance the communication quality.

Despite the benefits of OA-FL mentioned above, the limited service coverage of a single CS makes it challenging to access more devices [8]. In general, expanding service coverage by simply replicating CS inevitably results in significant energy consumption, construction investment, site support, leasing, and maintenance costs, making it a costly solution [9]. Additionally, due to user mobility, traffic on each CS experiences fluctuations, commonly known as the "tide effect."

[8]. These CS must be designed to handle maximum traffic rather than average traffic, resulting in a significant waste of processing resources and power during idle periods.

To address these issues, an effective solution is the MIMO Cloud-RAN architecture. This architecture consists of multiple access points (APs), also known as remote radio heads (RRHs), with each AP serving a specific set of mobile devices. These APs transmit (or receive) signals to (or from) mobile devices through a MIMO-based radio access network and upload (or download) data payloads to (or from) the CS via a fronthaul network [10]. MIMO Cloud-RAN provides flexible network planning and deployment [11], resulting in a significant increase in system coverage at a low cost. Furthermore, it enables the full utilization of idle processing resources and reduces the impact of the tide effect by centralizing computing resources into a resource pool of the CS.

In this paper, we introduce the OA-FL into MIMO Cloud-RAN and proposed a OA-FL in MIMO Cloud-RAN framework. More specifically, our proposed framework consists of three stages: edge aggregation, in which each AP aggregates local updates from edge devices through the MIMO-based radio access network [7] over the air to generate edge updates; global aggregation, in which the CS aggregates edge updates from APs through the fronthaul network to generate a global update; and model updating and broadcasting, in which the CS updates global model parameters and broadcasts it to every AP through the fronthaul network, which then broadcasts it to their served devices.

Additionally, we observed that the local updates in FL are typically correlated [12], resulting in correlated edge updates. This correlation, referred to as inter-AP correlation, can be leveraged to significantly reduce the communication cost of global aggregation. To better utilize the inter-AP correlation, we propose modeling the global aggregation stage as a lossy distributed source coding (L-DSC) problem to make analysis from the perspective of rate-distortion theory. Based on this analysis, we further analyze the performance of the proposed OA-FL in MIMO Cloud-RAN framework. Furthermore, we formulate a communication-learning optimization problem to improve the system performance by considering the inter-AP correlation. To solve this problem, we develop an algorithm by using alternating optimization (AO) and majorization-minimization (MM), which effectively improves the FL learning performance.

Subsequently, we propose a practical design that demonstrates the utilization of inter-AP correlation. Our design includes an encoding function and a joint decoding function, which enable efficient compression and reconstruction of the model updates. Specifically, the encoding

function consists of a compression module, quantization module, and error accumulation module, which work together to compress the edge update, add an error accumulation term, and quantize the resulting vector to satisfy the rate constraint. On the other hand, the decoding function utilizes a neural network structure to leverage inter-AP correlation for estimating the global update. The numerical results show that the proposed practical design effectively leverages inter-AP correlation, and outperforms other baseline schemes.

The remainder of this paper is structured as follows. In Section II, we provide an overview of the FL process and MIMO Cloud-RAN. In Section III, we present the OA-FL in MIMO Cloud-RAN framework. In Section IV, we make analysis for the L-DSC problem and the proposed OA-FL in MIMO Cloud-RAN framework. In Section V, we formulate an optimization problem for OA-FL in MIMO Cloud-RAN and develop an effective algorithm to solve it. In Section VI, we present a practical design, which exploits the inter-AP correlation. In Section VII, we validate proposed OA-FL in MIMO Cloud-RAN through experiments.

Notations: Throughout, regular small letters, regular capital letters, bold small letters, and bold capital letters denote scalars, random variables, vectors, and matrices, respectively. $(\cdot)^\dagger$, $(\cdot)^\top$ and $(\cdot)^H$ denote the conjugate, the transpose, and the conjugate transpose, respectively. \mathbb{R} and \mathbb{C} denote the real and complex number sets, respectively. $[k]$ denotes the integer set $\{1, \dots, k\}$. $[\mathbf{A}]_{k_1, k_2}$ denotes the k_1 -th row and k_2 -th column entry of matrix \mathbf{A} . Given the sets $\mathcal{K}_1 \subseteq [d_1]$, $\mathcal{K}_2 \subseteq [d_2]$, $[\mathbf{A}]_{\mathcal{K}_1, \mathcal{K}_2}$ denotes the $|\mathcal{K}_1| \times |\mathcal{K}_2|$ matrix obtained by removing all the (k_1, k_2) -th elements of \mathbf{A} with $k_1 \in [d_1] \setminus \mathcal{K}_1$ or $k_2 \in [d_2] \setminus \mathcal{K}_2$. When $\mathcal{K}_1 = \mathcal{K}_2 = \mathcal{K}$, $[\mathbf{A}]_{\mathcal{K}_1, \mathcal{K}_2}$ is simplified as $[\mathbf{A}]_{\mathcal{K}}$. $\mathcal{N}(\mu, \sigma^2)$ denotes normal distribution with mean μ and variance σ^2 . $\mathcal{CN}(\mu, \sigma^2)$ denotes the circularly-symmetric complex normal distribution with mean μ and covariance σ^2 . $\mathcal{N}(\boldsymbol{\mu}, \boldsymbol{\Sigma})$ denotes the multivariate normal distribution with mean vector $\boldsymbol{\mu}$ and covariance matrix $\boldsymbol{\Sigma}$. $\|\mathbf{x}\|$ denotes the l_2 norm of the vector \mathbf{x} . $\|\mathbf{A}\|$ denotes the induced 2-norm of the matrix \mathbf{A} . $\mathbf{0}$ or $\mathbf{1}$ denote all-zero or all-one vectors or matrices, respectively. \mathbf{I} denotes the identity matrix. $\nabla_{\mathbf{x}} = \frac{\partial}{\partial \mathbf{x}}$ denotes the gradient operator with respect to the vector \mathbf{x} . $\mathbb{E}[\cdot]$ denotes the expectation operator.

II. PRELIMINARIES

A. Federated Learning

We consider a wireless federated learning (FL) system, where N_D edge devices and a cloud server (CS) collaboratively learn a shared model based on the training data distributed over the

N_D edge devices. The objective is to minimize a global loss function $\mathcal{L}(\boldsymbol{\theta})$, i.e.,

$$\min_{\boldsymbol{\theta}} \mathcal{L}(\boldsymbol{\theta}) \triangleq \sum_{k \in [N_D]} \mathcal{L}_k(\boldsymbol{\theta}), \quad (1)$$

where vector $\boldsymbol{\theta} \in \mathbb{R}^N$ is the global model parameter vector with length N , and $\mathcal{L}_k(\boldsymbol{\theta})$ is the empirical loss of device k , defined by

$$\mathcal{L}_k(\boldsymbol{\theta}) = \sum_{\mathbf{b} \in \mathcal{B}_k} l(\boldsymbol{\theta}, \mathbf{b}), \quad (2)$$

where $l(\boldsymbol{\theta}, \mathbf{b})$ is the sample-wise loss function, \mathcal{B}_k is the local dataset of device k , and \mathbf{b} is a data sample of \mathcal{B}_k .

The minimization in (1) is typically solved by gradient descent (GD). Specifically, at each training round t , the model parameter $\boldsymbol{\theta}$ is updated via

$$\boldsymbol{\theta}^{(t+1)} = \boldsymbol{\theta}^{(t)} - \eta \nabla_{\boldsymbol{\theta}} \mathcal{L}(\boldsymbol{\theta}^{(t)}) = \boldsymbol{\theta}^{(t)} - \eta \sum_{k \in [N_D]} \mathbf{g}_k^{(t)}, \quad (3)$$

where $\eta \in \mathbb{R}$ is a predetermined learning rate, and $\mathbf{g}_k^{(t)} \triangleq \nabla_{\boldsymbol{\theta}} \mathcal{L}_k(\boldsymbol{\theta}^{(t)}) \in \mathbb{R}^N$ is the local update uploaded from each device k to the CS over an uplink channel. After that, $\boldsymbol{\theta}^{(t+1)}$ is broadcast to all the devices by the CS over a downlink channel to synchronize the learning model among the devices. The above process continues until it converges.

B. MIMO Cloud-RAN

In this paper, we consider the deployment of the above FL over a cloud-computing-based architecture for cellular networks, termed MIMO Cloud-RAN [13]. This architecture consists of multiple access points (APs), also known as remote radio heads (RRHs). Each AP serves an individual set of mobile devices. These APs transmit (or receive) signals to (or from) mobile devices through a MIMO-based radio access network, and uploads (or downloads) the data payload to (or from) the CS via a fronthaul network, as depicted in Fig. 1. Details are given below.

- 1) Uplink radio access network: The uplink radio access network is a MIMO MAC channel, where each AP is equipped with N_R antennas, and each terminal device with N_T antennas. We assume block-fading, i.e., the channel state information (CSI) keeps invariant during a training round. Let C be the number of uplink channel uses in a training round. Then the received signal matrix at AP i in the t -th round is expressed as

$$\mathbf{Y}_i^{(t)} = \sum_{k \in \mathcal{N}_{D,i}} \mathbf{H}_{ik}^{(t)} \mathbf{X}_k^{(t)} + \mathbf{Z}_i^{(t)} \in \mathbb{R}^{N_R \times C}, \forall i \in [N_A], \quad (4)$$

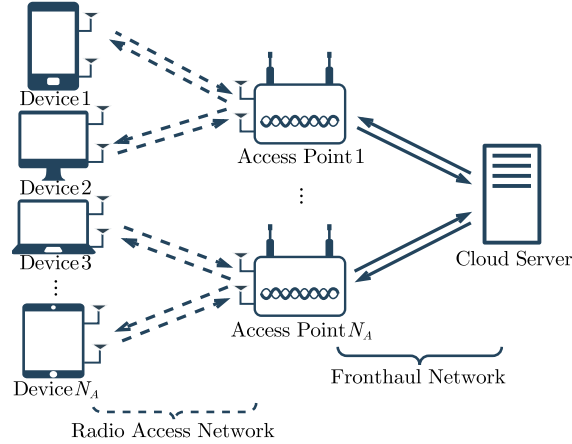


Fig. 1. An illustration of the MIMO Cloud-RAN.

where $\mathbf{X}_k^{(t)} \in \mathbb{C}^{N_T \times C}$ is the signal matrix transmitted by device k , $\mathbf{H}_{ik}^{(t)} \in \mathbb{C}^{N_R \times N_T}$ is the channel matrix between device k and AP i ¹, $\mathbf{Z}_i^{(t)} \in \mathbb{C}^{N_R \times C}$ is an additive white Gaussian noise (AWGN) matrix whose entries are independently drawn from $\mathcal{CN}(0, \sigma_z^{(t)2})$, and $\mathcal{N}_{D,i}$ is the set of devices served by AP i satisfying $\mathcal{N}_{D,1} \cup \dots \cup \mathcal{N}_{D,N_A} = [N_D]$ and $\mathcal{N}_{D,i} \cap \mathcal{N}_{D,j} = \emptyset, \forall i \neq j$. Note that the sum in (4) implies that signals $\{\mathbf{X}_k^{(t)}\}_{k \in \mathcal{N}_{D,i}}$ are transmitted over shared radio resources and are synchronized among devices². This enables the utilization of the superposition characteristic of electromagnetic waves for signal aggregation, a.k.a., over-the-air computation.

- 2) Uplink fronthaul network: The uplink fronthaul network relies on dedicated fibers for data delivery [10]. Specifically, each AP i transmits its signals to the CS via a rate-constrained wired link.
- 3) Downlink fronthaul network: Similarly, in the downlink fronthaul network, the CS broadcasts its signals to every AP via a rate-constrained wired link.
- 4) Downlink radio access network: The downlink radio access network associated with each AP i is a MIMO broadcast channel, i.e., the downlink dual of the MIMO MAC in (4). In each training round t , each AP i broadcasts its signals to every device in $\mathcal{N}_{D,i}$.

¹The CSI $\{\mathbf{H}_{ik}\}_{k \in \mathcal{N}_{D,i}, \forall i \in [N_A]}$ is estimated at each AP i via channel training [14], [15].

²The synchronization can be realized by using the existing techniques, e.g., the timing-advance mechanism for uplink synchronization in 4G Long Term Evolution (LTE) [16].

III. OA-FL IN MIMO CLOUD-RAN

We now describe the FL process deployed in the MIMO Cloud-RAN system. As depicted in Fig. 2, the OA-FL in MIMO Cloud-RAN framework consists of three stages: (i) edge aggregation; (ii) global aggregation; and (iii) model updating and broadcasting.

A. Edge Aggregation

We start with the edge aggregation stage of the proposed framework, where each AP aggregates local updates from N_D devices through the uplink radio access network in an over-the-air fashion. Specifically, at the t -th round, each device k first normalizes its local update $\mathbf{g}_k^{(t)}$ by

$$\tilde{\mathbf{g}}_k^{(t)} = \left(\mathbf{g}_k^{(t)} - \bar{g}_k^{(t)} \mathbf{1} \right) / \sqrt{v_k^{(t)}} \in \mathbb{R}^N, \forall k \in [N_D], \quad (5)$$

where $v_k^{(t)} = \frac{1}{N} \left\| \mathbf{g}_k^{(t)} - \bar{g}_k^{(t)} \mathbf{1} \right\|^2$ and $\bar{g}_k^{(t)} = \frac{1}{N} \sum_{n \in [N]} \left[\mathbf{g}_k^{(t)} \right]_n$ ³. To match the complex communication system in (4), each device k maps $\tilde{\mathbf{g}}_k$ to a complex vector $\mathbf{r}_k \in \mathbb{C}^C$, defined as

$$\text{Re}\{\mathbf{r}_k^{(t)}\} \triangleq [\tilde{g}_{k,1}^{(t)}, \dots, \tilde{g}_{k,N/2}^{(t)}]^\top, \quad \text{Im}\{\mathbf{r}_k^{(t)}\} \triangleq [\tilde{g}_{k,N/2+1}^{(t)}, \dots, \tilde{g}_{k,N}^{(t)}]^\top, \quad (6)$$

where $\tilde{g}_{k,m}^{(t)}$ is the m -th entry of $\tilde{\mathbf{g}}_k^{(t)}$, and $C = \frac{N}{2}$. Then each device k transmits $\mathbf{r}_k^{(t)}$ with C channel uses, i.e., the transmitted signal matrix of device k is given by

$$\mathbf{X}_k^{(t)} \triangleq \boldsymbol{\alpha}_k^{(t)} \mathbf{r}_k^{(t)\top} \in \mathbb{C}^{N_T \times C}, \forall k \in [N_D], \quad (7)$$

where $\boldsymbol{\alpha}_k^{(t)} \in \mathbb{C}^{N_T}$ is transmit beamforming vector of device k with N_T being the number of transmit antennas. Let $r_{k,c}^{(t)}$ be the c -th entry of $\mathbf{r}_k^{(t)}$ and $\mathbf{x}_{k,c}^{(t)} \in \mathbb{C}^{N_T}$ be the c -th col of $\mathbf{X}_k^{(t)}$. The transmitted signal of the device k at the c -th channel use is given by $\mathbf{x}_{k,c}^{(t)} = r_{k,c}^{(t)} \boldsymbol{\alpha}_k^{(t)}$, satisfying the power constraint of

$$\mathbb{E} \left[\left\| \mathbf{x}_{k,c}^{(t)} \right\|^2 \right] = 2 \left\| \boldsymbol{\alpha}_k^{(t)} \right\|^2 \leq P_k^{(t)}, \forall k \in [N_D], \forall n \in [N], \quad (8)$$

where the equality is from (5) (implying $\mathbb{E}[|r_{k,c}^{(t)}|^2] = 2$), and P_k is the power budget of device k . After transmitting the signal matrices $\{\mathbf{X}_k^{(t)}\}_{k \in \mathcal{N}_{D,i}}$ to AP i via the uplink radio access network in (4), AP i applies a receive beamforming vector to combine the received signal matrix $\mathbf{Y}_i^{(t)}$ over the air, resulting in $\hat{\mathbf{r}}_i^{(t)}$ as

$$\hat{\mathbf{r}}_i^{(t)} = \left(\boldsymbol{\beta}_i^{(t)\text{H}} \mathbf{Y}_i^{(t)} \right)^\top = \sum_{k \in \mathcal{N}_{D,i}} \mathbf{r}_k^{(t)} \left(\boldsymbol{\beta}_i^{(t)\text{H}} \mathbf{H}_{ik}^{(t)} \boldsymbol{\alpha}_k^{(t)} \right)^\top + \mathbf{Z}_i^{(t)\top} \boldsymbol{\beta}_i^{(t)\dagger} \in \mathbb{C}^C, \forall i \in [N_A], \quad (9)$$

³We assume that the CS perfectly knows $\bar{g}_k^{(t)}$ and $v_k^{(t)}$. In practice, the cost of transmitting the scalars $\{\bar{g}_k^{(t)}, v_k^{(t)}\}_{k \in [N_D]}$ to the CS is negligible as compared to the overall cost.

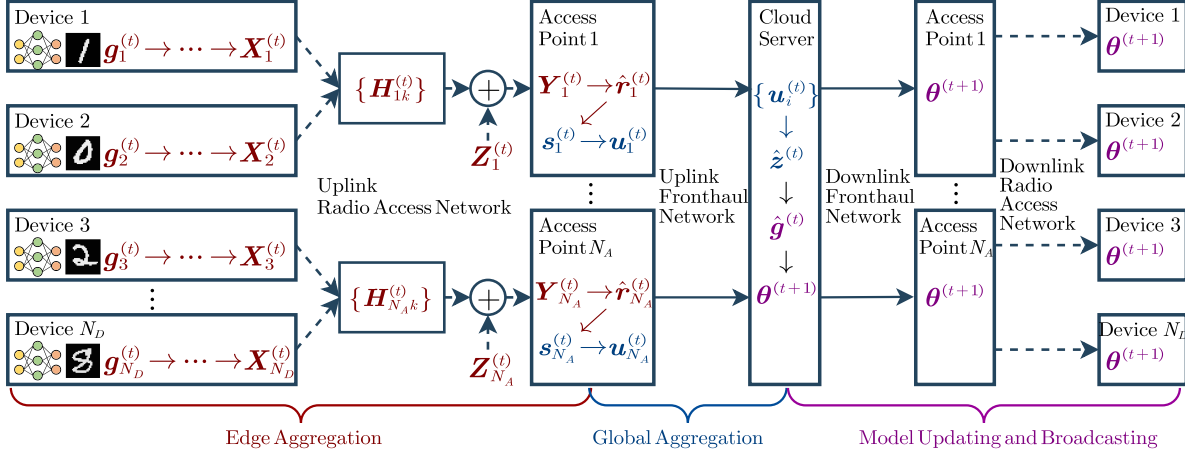


Fig. 2. An illustration of a training round of MIMO Cloud-RAN based OA-FL.

where $\beta_i^{(t)} \in \mathbb{C}^{N_R}$ is the receive beamforming vector of AP i . Then each AP i constructs its edge update as

$$\mathbf{s}_i^{(t)} \triangleq \left[\text{Re} \left\{ \hat{\mathbf{r}}_i^{(t)} \right\}^T, \text{Im} \left\{ \hat{\mathbf{r}}_i^{(t)} \right\}^T \right]^T \in \mathbb{R}^N, \forall i \in [N_A]. \quad (10)$$

B. Global Aggregation

We now describe the global aggregation stage of our proposed framework, where the CS aggregates edge updates from N_A APs through the uplink fronthaul network. Specifically, at the t -th round, each AP i encodes $\mathbf{s}_i^{(t)}$ to a vector

$$\mathbf{u}_i^{(t)} = f_i^{(t)} \left(\mathbf{s}_i^{(t)} \right) \in [B_i^{(t)}], \forall i \in [N_A], \quad (11)$$

where $f_i^{(t)} : \mathbb{R}^N \rightarrow [B_i^{(t)}], \forall i \in [N_A]$ is an encoding function, and $B_i^{(t)}$ is the codebook size of $f_i^{(t)}$. Then each AP transmits $\mathbf{u}_i^{(t)}$ to the CS over the uplink fronthaul network. Upon receiving the signals $\{\mathbf{u}_i^{(t)}\}_{i \in [N_A]}$, the CS aggregates (or alternatively, decodes) them as a global update.

$$\hat{\mathbf{z}}^{(t)} = f^{(t)} \left(\mathbf{u}_1^{(t)}, \dots, \mathbf{u}_{N_A}^{(t)} \right) \in \mathbb{R}^N, \quad (12)$$

where $f^{(t)} : [B_1^{(t)}] \times \dots \times [B_{N_A}^{(t)}] \rightarrow \mathbb{R}^N$ is a decoding function. Local updates in FL are typically correlated [12], resulting in correlated edge updates. This correlation, called inter-AP correlation, can be exploited to significantly reduce the communication cost of global aggregation. To improve communication efficiency, we treat global aggregation as a lossy distributed source coding (L-DSC) process. In L-DSC, given an aggregation target function $\kappa : \underbrace{\mathbb{R}^N \times \dots \times \mathbb{R}^N}_{N_A} \rightarrow \mathbb{R}^N$ and a

distortion measure function $d : \mathbb{R}^N \times \mathbb{R}^N \rightarrow \mathbb{R}_+$, an achievable rate-distortion tuple is defined below.

Definition 1. A rate-distortion tuple $(R_1^{(t)}, \dots, R_{N_A}^{(t)}, D^{(t)})$, $\forall t$ is said to be achievable if for any $\epsilon > 0$ and any sufficiently large N , there exists N_A encoding functions $\{f_i^{(t)}\}_{i=1}^{N_A}$ and a joint decoding function $f^{(t)}$ such that rate $\frac{1}{N} \log(B_i^{(t)}) \leq R_i^{(t)} + \epsilon$, $\forall i \in [N_A]$, and expected aggregation distortion $\frac{1}{N} \mathbb{E} [d(\mathbf{z}^{(t)}, \hat{\mathbf{z}}^{(t)})] \leq D^{(t)} + \epsilon$, where $\mathbf{z}^{(t)} \triangleq \kappa(\mathbf{s}_1^{(t)}, \dots, \mathbf{s}_{N_A}^{(t)})$.

Loosely speaking, as the model dimension N increases, the expected distortion $\frac{1}{N} \mathbb{E} [d(\mathbf{z}^{(t)}, \hat{\mathbf{z}}^{(t)})]$ can be arbitrarily close to $D^{(t)}$, when the rate $\frac{1}{N} \log(B_i^{(t)})$ tends to $R_i^{(t)}$, $\forall i \in [N_A]$. The rate-distortion region of L-DSC is defined as the set of all achievable rate-distortion tuples, denoted by $\mathcal{RD}^{(t)}$. Detailed analysis of L-DSC will be provided later in Section IV-A.

Algorithm 1 OA-FL in MIMO Cloud-RAN.

- 1: **At each training round t**
 - 2: **Edge aggregation:**
 - 3: Each device k computes its local update $\mathbf{g}_k^{(t)}$ with \mathcal{B}_k and $\boldsymbol{\theta}$
 - 4: Each device k computes $\mathbf{X}_k^{(t)}$ from $\mathbf{g}_k^{(t)}$ via (5)-(7)
 - 5: Each device k transmits $\mathbf{X}_k^{(t)}$ to the APs via the channel in (4)
 - 6: Each AP i receives the matrix $\mathbf{Y}_i^{(t)}$ and computes $\mathbf{s}_i^{(t)}$ via (9)-(10)
 - 7: **Global aggregation:**
 - 8: Each AP i computes $\mathbf{u}_i^{(t)}$ from $\mathbf{s}_i^{(t)}$ via (11)
 - 9: Each AP i transmits $\mathbf{u}_i^{(t)}$ to the CS
 - 10: The CS receives $\{\mathbf{u}_i^{(t)}\}_{i=1}^{N_A}$ and computes $\hat{\mathbf{z}}^{(t)}$ via (12)
 - 11: **Model updating and broadcast:**
 - 12: The CS computes $\hat{\mathbf{g}}^{(t)}$ from $\hat{\mathbf{z}}^{(t)}$ via (13) and updates $\boldsymbol{\theta}^{(t)}$ via (14)
 - 13: The CS broadcasts $\boldsymbol{\theta}^{(t+1)}$ to all the APs
 - 14: Each AP i broadcasts the received $\boldsymbol{\theta}^{(t+1)}$ to every device in $\mathcal{N}_{D,i}$
-

C. Model Updating and Broadcasting

We now describe the model updating and broadcasting stage of our proposed framework. Specifically, the CS computes the vector $\hat{\mathbf{g}}^{(t)} \in \mathbb{R}^N$ as

$$\hat{\mathbf{g}}^{(t)} = \hat{\mathbf{z}}^{(t)} + \sum_{k \in [N_D]} \bar{g}_k^{(t)} \mathbf{1} \in \mathbb{R}^N, \quad (13)$$

where the bias term $\sum_{k \in [N_D]} \bar{g}_k^{(t)}$ given in (5) is known at the CS through error-free transmission. Then the CS updates the global model as

$$\boldsymbol{\theta}^{(t+1)} = \boldsymbol{\theta}^{(t)} - \eta \hat{\mathbf{g}}^{(t)}, \quad (14)$$

where η is given in (3). Then the CS broadcasts the global model $\boldsymbol{\theta}^{(t+1)}$ to every AP via the downlink fronthaul network described in Section II-B. Next each AP i broadcasts received $\boldsymbol{\theta}^{(t+1)}$ to every device in $\mathcal{N}_{D,i}$. Following the common practice in [12], [17]–[20], we assume that the broadcast process in the downlink fronthaul network and the downlink radio access network is error-free. The overall scheme of OA-FL in MIMO Cloud-RAN is summarized in Algorithm 1.

IV. PERFORMANCE ANALYSIS

In this section, we first analyze the L-DSC problem described in Section III-B, and then carry out the performance analysis of the MIMO Cloud-RAN based OA-FL, yielding an upper bound on the learning performance.

A. Preliminaries

Recall that we model global aggregation as an L-DSC process. We define the rate-distortion region $\mathcal{RD}^{(t)}$ as the set of all achievable rate-distortion tuples in L-DSC at the t -th training round. However, this region is generally unknown. To establish a tractable inner region of $\mathcal{RD}^{(t)}$, we rely on the following assumptions.

Assumption 1. Denote a matrix $\boldsymbol{\Sigma}_S^{(t)} \in \mathbb{R}^{N_A \times N_A}$ with $[\boldsymbol{\Sigma}_S^{(t)}]_{i,j} = \frac{1}{N} \mathbb{E} \left[(\mathbf{s}_i^{(t)})^\top \mathbf{s}_j^{(t)} \right], \forall i, j \in [N_A]$. Denote the n -th entry of $\mathbf{s}_i^{(t)}$ as $s_{i,n}^{(t)}$. For the edge updates $\{\mathbf{s}_i^{(t)}\}_{i \in [N_A]}$, we assume that (i) $s_{i,n}^{(t)} \sim \mathcal{N}(0, [\boldsymbol{\Sigma}_S^{(t)}]_{i,i}), \forall i \in [N_A], \forall n \in [N]$, and (ii) $(s_{1,n}^{(t)}, s_{2,n}^{(t)}, \dots, s_{N_A,n}^{(t)}) \sim \mathcal{N}(\mathbf{0}, \boldsymbol{\Sigma}_S^{(t)}), \forall n \in [N]$.

Assumption 1 allows us to treat $\{s_{1,n}^{(t)}, \dots, s_{N_A,n}^{(t)}\}_{n \in [N]}$ as N samples generated from an N_A -component memoryless Gaussian source $\mathcal{N}(\mathbf{0}, \Sigma_S^{(t)})^4$. Based on Assumption 1, we provide an inner region of $\mathcal{RD}^{(t)}$ as follows:

Lemma 1. *Under the quadratic distortion measure $d(\mathbf{a}^{(t)}, \mathbf{b}^{(t)}) = \|\mathbf{a}^{(t)} - \mathbf{b}^{(t)}\|^2$ and the linear aggregation target $\kappa(\mathbf{a}_1^{(t)}, \dots, \mathbf{a}_{N_A}^{(t)}) = \sum_{i=1}^{N_A} c_i^{(t)} \mathbf{a}_i^{(t)}$, where $c_i^{(t)}$ is the i -th entry of a weighted coefficient vector $\mathbf{c}^{(t)} \in \mathbb{R}^{N_A}$, it is concluded from Assumption 1 that*

$$\begin{aligned} \mathcal{RD}_{in}^{(t)} = \bigcup_{\Sigma_V^{(t)}} \left\{ \left(R_1^{(t)}, \dots, R_{N_A}^{(t)}, D^{(t)} \right) : \right. \\ (i) \sum_{i \in \mathcal{K}} R_i^{(t)} \geq \frac{1}{2} \log \left(\frac{\det(\Sigma_S^{(t)} + \Sigma_V^{(t)})}{\det([\Sigma_S^{(t)}]_{\mathcal{K}^c} + [\Sigma_V^{(t)}]_{\mathcal{K}^c}) \det([\Sigma_V^{(t)}]_{\mathcal{K}})} \right), \forall \mathcal{K} \subset [N_A], \mathcal{K} \neq \emptyset; \\ (ii) \sum_{i \in [N_A]} R_i^{(t)} \geq \frac{1}{2} \log \left(\frac{\det(\Sigma_S^{(t)} + \Sigma_V^{(t)})}{\det(\Sigma_V^{(t)})} \right); \\ (iii) D^{(t)} \geq \frac{1}{N} \mathbb{E}[\|\mathbf{z}^{(t)} - \hat{\mathbf{z}}^{(t)}\|^2] \left. \right\}, \end{aligned} \quad (15)$$

where $\mathcal{RD}_{in}^{(t)} \subset \mathcal{RD}^{(t)}$, rate $R_i^{(t)}, \forall i$ and distortion $D^{(t)}$ are given in Definition 1, $\hat{\mathbf{z}}$ is given in (12), $\mathbf{z}^{(t)} \triangleq \kappa(\mathbf{s}_1^{(t)}, \dots, \mathbf{s}_{N_A}^{(t)})$, $\Sigma_V^{(t)} \in \mathbb{R}^{N_A \times N_A}$ is an undetermined diagonal matrix called L-DSC parameter, and $\frac{1}{N} \mathbb{E}[\|\mathbf{z}^{(t)} - \hat{\mathbf{z}}^{(t)}\|^2] \triangleq \mathbf{c}^{(t)\top} \Sigma_S^{(t)} \mathbf{c}^{(t)} - \mathbf{c}^{(t)\top} \Sigma_S^{(t)} (\Sigma_S^{(t)} + \Sigma_V^{(t)})^{-1} \Sigma_S^{(t)} \mathbf{c}^{(t)}$.

Proof. See the proof in [20]. □

We emphasize that the choice of L-DSC parameter $\Sigma_V^{(t)}$ leads to different codebooks for L-DSC. By tuning the L-DSC parameter $\Sigma_V^{(t)}$, we search for the rate-distortion tuple in $\mathcal{RD}_{in}^{(t)}$ that minimizes the distortion $\mathbb{E}[\|\mathbf{z}^{(t)} - \hat{\mathbf{z}}^{(t)}\|^2]$. However, due to the link rate-constraints, $\Sigma_V^{(t)}$ cannot be chosen arbitrarily. Let $r_i^{(t)}$ denote the maximum information rate that AP i can transmit to the CS at the training round t . To ensure reliable uplink transmission, the (source coding) rates in Lemma 1 must satisfy

$$R_i^{(t)} \leq r_i^{(t)}, \forall i \in [N_A]. \quad (16)$$

⁴The matrix Σ_S models correlations among APs, and is either known a priori or estimated during training. A simple approach is for each AP to send a sub-vector of \mathbf{s}_i to the CS intermittently for parameter estimation during training.

B. Communication Error Analysis of OA-FL in MIMO Cloud-RAN

We now analyze the communication error in the OA-FL in MIMO Cloud-RAN framework. The gradient aggregation error at the t -th training round is given by

$$\mathbf{e}^{(t)} = \nabla \mathcal{L}(\boldsymbol{\theta}^{(t)}) - \hat{\mathbf{g}}^{(t)} \in \mathbb{R}^N, \quad (17)$$

where $\nabla \mathcal{L}(\boldsymbol{\theta}^{(t)})$ is from (3) and $\hat{\mathbf{g}}^{(t)}$ is from (14). From (5)-(13), we see that the error \mathbf{e} mainly arises from the transmission in the uplink radio access network, and the transmission in the uplink fronthaul network. Correspondingly, we decompose the error \mathbf{e} into two terms as

$$\mathbf{e}^{(t)} = \sum_{k \in [N_D]} \mathbf{g}_k^{(t)} - \sum_{k \in [N_D]} \bar{\mathbf{g}}_k^{(t)} \mathbf{1} - \hat{\mathbf{z}}^{(t)} \quad (18a)$$

$$= \underbrace{\sum_{k \in [N_D]} \sqrt{v_k^{(t)}} \bar{\mathbf{g}}_k^{(t)} - \sum_{i \in [N_A]} [\mathbf{c}^{(t)}]_i \mathbf{s}_i^{(t)}}_{\text{Wireless transmission error}} + \underbrace{\mathbf{z}^{(t)} - \hat{\mathbf{z}}^{(t)}}_{\text{Wired transmission error}} \quad (18b)$$

$$= \mathbf{e}_1^{(t)} + \mathbf{e}_2^{(t)} \in \mathbb{R}^N, \quad (18c)$$

where the first equality is from (13), the second equality is from (5), $\mathbf{e}_1^{(t)} \in \mathbb{R}^N$ is the wireless transmission error caused by the communication noise in (4), and $\mathbf{e}_2^{(t)} \in \mathbb{R}^N$ is the wired transmission error caused by the rate-constraint in the fronthaul network. We analyze the bound of $\mathbb{E}[\|\mathbf{e}^{(t)}\|^2]$ in the following lemma.

Lemma 2. Assume $\frac{1}{N} \mathbb{E}[\|(\tilde{\mathbf{g}}_{k_1}^{(t)})^H \tilde{\mathbf{g}}_{k_2}^{(t)}\|^2] = [\boldsymbol{\Sigma}_S^{(t)}]_{i_1, i_2}, \forall k_1 \in \mathcal{N}_{D, i_1}, k_2 \in \mathcal{N}_{D, i_2}$. Then

$$\mathbb{E}[\|\mathbf{e}^{(t)}\|^2] \leq 2ND_{\text{system}}^{(t)},$$

where

$$\begin{aligned} D_{\text{system}}^{(t)} &\triangleq \sum_{i_1 \in [N_A]} \sum_{i_2 \in [N_A]} [\boldsymbol{\Sigma}_S^{(t)}]_{i_1, i_2} \sum_{k \in \mathcal{N}_{D, i_1}} \left(\sqrt{v_k^{(t)}} - c_{i_1}^{(t)} \boldsymbol{\alpha}_k^{(t)\top} \mathbf{H}_{i_1 k}^{(t)\top} \boldsymbol{\beta}_{i_1}^{(t)\dagger} \right)^H \\ &\times \sum_{k \in \mathcal{N}_{D, i_2}} \left(\sqrt{v_k^{(t)}} - c_{i_2}^{(t)} \boldsymbol{\alpha}_k^{(t)\top} \mathbf{H}_{i_2 k}^{(t)\top} \boldsymbol{\beta}_{i_2}^{(t)\dagger} \right) + \sum_{i \in [N_A]} \varepsilon_i^{(t)} c_i^{(t)2} \|\boldsymbol{\beta}_i^{(t)}\|^2 \\ &+ \mathbf{c}^{(t)\top} \boldsymbol{\Sigma}_S^{(t)} \mathbf{c}^{(t)} - \mathbf{c}^{(t)\top} \boldsymbol{\Sigma}_S^{(t)} \left(\boldsymbol{\Sigma}_S^{(t)} + \boldsymbol{\Sigma}_V^{(t)} \right)^{-1} \boldsymbol{\Sigma}_S^{(t)\top} \mathbf{c}^{(t)} \in \mathbb{R}, \end{aligned} \quad (19)$$

the matrices $\boldsymbol{\Sigma}_S^{(t)}$ and $\boldsymbol{\Sigma}_V^{(t)} \in \mathbb{R}^{N_A \times N_A}$ are given in Assumption 1, $\varepsilon_i \triangleq \frac{1}{N} \mathbb{E}[\|\mathbf{z}_i^{(t)}\|^2] \in \mathbb{R}, \forall i \in [N_A]$ is the noise power⁵, $\boldsymbol{\alpha}_k^{(t)}, \boldsymbol{\beta}_i^{(t)}, \mathbf{H}_{ik}^{(t)}, \forall i, k, t$ are given in (4), $\mathbf{c}^{(t)}$ is given in Lemma 1, and $\{v_k^{(t)}\}_{k=1}^{N_D}$ are given in (5).

⁵The noise power ε_i is estimated at each AP i by the expectation-maximization algorithm [21].

Proof. See Appendix A. □

C. Convergence Analysis of OA-FL in MIMO Cloud-RAN

We now present convergence analysis to establish the relationship between the FL convergence rate and the communication error (17). Following [22], we introduce standard assumptions in stochastic optimization below.

Assumption 2. (i) $\mathcal{L}(\cdot)$ is strongly convex with some (positive) parameter μ . That is, $\mathcal{L}(\mathbf{y}) \geq \mathcal{L}(\mathbf{x}) + (\mathbf{y} - \mathbf{x})^T \nabla \mathcal{L}(\mathbf{x}) + \frac{\mu}{2} \|\mathbf{y} - \mathbf{x}\|^2, \forall \mathbf{x}, \mathbf{y} \in \mathbb{R}^N$. (ii) The gradient $\nabla \mathcal{L}(\cdot)$ is Lipschitz continuous with some (positive) parameter L . That is, $\|\nabla \mathcal{L}(\mathbf{x}) - \nabla \mathcal{L}(\mathbf{y})\| \leq L \|\mathbf{x} - \mathbf{y}\|, \forall \mathbf{x}, \mathbf{y} \in \mathbb{R}^N$. (iii) $\mathcal{L}(\cdot)$ is twice continuously differentiable. (iv) The gradient with respect to any training sample, denoted by $\nabla l(\boldsymbol{\theta}; \cdot)$, is upper bounded at $\boldsymbol{\theta}$ as $\|\nabla l(\boldsymbol{\theta}, \mathbf{b})\|^2 \leq \gamma_1 + \gamma_2 \|\nabla \mathcal{L}(\boldsymbol{\theta})\|^2$, where \mathbf{b} is a data sample from the whole datasets $\{\mathcal{B}_k\}_{k=1}^{N_D}$, and $\gamma_1 \geq 0, \gamma_2 > 0$ are some constants.

Assumption 2-(i) ensures that a global optimum exists for the loss function $\mathcal{L}(\cdot)$. Assumption 2-(ii) is imposed on the gradient function $\nabla \mathcal{L}(\cdot)$ to prevent the function value from changing too fast, so as to construct a more robust machine learning model. Assumption 2-(iv) provides a bound on the norm of the local gradients, i.e., \mathbf{g}_k . Assumption 2 leads to an upper bound on the loss function $\mathcal{L}(\boldsymbol{\theta}^{(t+1)})$ with respect to the model updating (14), as given in the following lemma.

Lemma 3. Assume that $\mathcal{L}(\cdot)$ satisfies Assumption 2, at the t -th training round with the learning rate η is set to $1/L$. Then

$$\mathbb{E}[\mathcal{L}(\boldsymbol{\theta}^{(t+1)})] \leq \mathbb{E}[\mathcal{L}(\boldsymbol{\theta}^{(t)})] - \frac{1}{2L} \mathbb{E}[\|\nabla \mathcal{L}(\boldsymbol{\theta}^{(t)})\|^2] + \frac{1}{2L} \mathbb{E}[\|\mathbf{e}^{(t)}\|^2], \quad (20)$$

where the Lipschitz constant L is given in Assumption 2- (ii).

Proof. See [22, Lemma 2.1]. □

We are now ready to present an upper bound of the expected difference between the training loss and the optimal loss at round $t + 1$, i.e., $\mathbb{E}[\mathcal{L}(\boldsymbol{\theta}^{(t+1)}) - \mathcal{L}(\boldsymbol{\theta}^*)]$.

Theorem 1. Based on Assumption 2, the loss function at the t -th round $\mathcal{L}(\boldsymbol{\theta})^{(t)}$ satisfies

$$\mathbb{E}[\mathcal{L}(\boldsymbol{\theta}^{(t+1)})] - \mathbb{E}[\mathcal{L}(\boldsymbol{\theta}^*)] \leq \left(1 - \frac{\mu}{L}\right)^t (\mathbb{E}[\mathcal{L}(\boldsymbol{\theta}^{(1)})] - \mathbb{E}[\mathcal{L}(\boldsymbol{\theta}^*)]) + \sum_{t'=1}^t \left(1 - \frac{\mu}{L}\right)^{t-t'} \frac{N}{L} D_{\text{system}}^{(t')}, \quad (21)$$

where $(\cdot)^t$ denotes the t -th power operator, $\mathcal{L}(\cdot)$ is the total empirical loss function given in (1), $\boldsymbol{\theta}^{(1)}$ is the initial system model parameter, and $D_{\text{system}}^{(t)}$ is given in Lemma 2.

Proof. From [22, eq. (2.4)], we have

$$\mathbb{E}[\|\nabla\mathcal{L}(\boldsymbol{\theta}^{(t)})\|^2] \geq 2\mu(\mathbb{E}[\mathcal{L}(\boldsymbol{\theta}^{(t)})] - \mathbb{E}[\mathcal{L}(\boldsymbol{\theta}^{(*)})]). \quad (22)$$

Subtracting $\mathbb{E}[\mathcal{L}(\boldsymbol{\theta}^{(*)})]$ on both sides of (20) in Lemma 3 and plugging (22) and Lemma 2 into (20), we obtain

$$\mathbb{E}[\mathcal{L}(\boldsymbol{\theta}^{(t+1)})] - \mathbb{E}[\mathcal{L}(\boldsymbol{\theta}^{(*)})] \leq \left(1 - \frac{\mu}{L}\right) (\mathbb{E}[\mathcal{L}(\boldsymbol{\theta}^{(t)})] - \mathbb{E}[\mathcal{L}(\boldsymbol{\theta}^{(*)})]) + \frac{N}{L} D_{\text{system}}^{(t)}. \quad (23)$$

Applying the above inequality recursively yields (21), which completes the proof. \square

From Theorem 1, we see that $\mathbb{E}[\mathcal{L}(\boldsymbol{\theta}^{(t)}) - \mathcal{L}(\boldsymbol{\theta}^{(*)})]$, i.e., the expected difference between the training loss and the optimal loss at the t -th round, is upper bounded by the right-hand side of the inequality in (21). Moreover, this upper bound converges with speed $1 - \frac{\mu}{L}$, since $\frac{\mu}{L} > 0$. Empirically, we find that our proposed scheme always converges with appropriately chosen system parameters. The following corollary further characterizes the convergence behavior of $\mathbb{E}[\mathcal{L}(\boldsymbol{\theta}^{(t+1)}) - \mathcal{L}(\boldsymbol{\theta}^{(*)})]$.

Corollary 1. *As $t \rightarrow \infty$, we have*

$$\lim_{t \rightarrow \infty} \mathbb{E}[\mathcal{L}(\boldsymbol{\theta}^{(t+1)}) - \mathcal{L}(\boldsymbol{\theta}^{(*)})] \leq \sum_{t'=1}^t \left(1 - \frac{\mu}{L}\right)^{t-t'} \frac{N}{L} D_{\text{system}}^{(t')} \quad (24)$$

Proof. By noting $\frac{\mu}{L} > 0$, we have $\lim_{t \rightarrow \infty} (1 - \frac{\mu}{L})^t = 0$. Plugging this result into (21), we obtain (24). \square

Corollary 1 shows that our proposed scheme guarantees to converge. However, there generally exists a gap between the converged loss $\lim_{t \rightarrow \infty} \mathbb{E}[\mathcal{L}(\boldsymbol{\theta}^{(t+1)})]$ and the optimal one $\mathbb{E}[\mathcal{L}(\boldsymbol{\theta}^{(*)})]$ because of the communication error. Therefore, we next aim to minimize the gap, so as to optimize our proposed framework.

V. SYSTEM OPTIMIZATION

A. Problem Formulation

From Theorem 1 and Corollary 1, the upper bound $\sum_{t'=1}^t \left(1 - \frac{\mu}{L}\right)^{t-t'} \frac{N}{L} D_{\text{system}}^{(t')}$ in (24) represents the impact of the wireless transmission error and the wired transmission error on the asymptotic learning performance. Specifically, a smaller $\sum_{t'=1}^t \left(1 - \frac{\mu}{L}\right)^{t-t'} \frac{N}{L} D_{\text{system}}^{(t')}$ leads to a smaller

gap in $\lim_{t \rightarrow \infty} \mathbb{E}[\mathcal{L}(\boldsymbol{\theta}^{(t+1)}) - \mathcal{L}(\boldsymbol{\theta}^{(*)})]$. This motivates us to use $\sum_{t'=1}^t (1 - \frac{\mu}{L})^{t-t'} \frac{N}{L} D_{\text{system}}^{(t')}$ as the performance metric of our proposed framework, i.e., to minimize $D_{\text{system}}^{(t)}$ in Theorem 1 over $\{\boldsymbol{\beta}_i^{(t)}\}_{i=1}^{N_A}$, $\{\boldsymbol{\alpha}_k^{(t)}\}_{k=1}^{N_D}$, $\boldsymbol{\Sigma}_V^{(t)}$ and $\mathbf{c}^{(t)}$ at each round t . Since the optimization problem takes the same form over rounds, we simplify the notation by omitting the index t , and formulate the design problem as follows:

$$\begin{aligned} \underset{\boldsymbol{\Sigma}_V, \mathbf{c}, \{\boldsymbol{\beta}_i\}_{i=1}^{N_A}, \{\boldsymbol{\alpha}_k\}_{k=1}^{N_D}}{\text{minimize}} \quad & \sum_{i_1 \in [N_A]} \sum_{i_2 \in [N_A]} [\boldsymbol{\Sigma}_S]_{i_1, i_2} \sum_{k \in \mathcal{N}_{D, i_1}} (\sqrt{v_k} - c_{i_1} \boldsymbol{\alpha}_k^\top \mathbf{H}_{i_1 k}^\top \boldsymbol{\beta}_{i_1}^\dagger)^H \\ & \times \sum_{k \in \mathcal{N}_{D, i_2}} (\sqrt{v_k} - c_{i_2} \boldsymbol{\alpha}_k^\top \mathbf{H}_{i_2 k}^\top \boldsymbol{\beta}_{i_2}^\dagger) + \sum_{i \in [N_A]} \varepsilon_i c_i^2 \|\boldsymbol{\beta}_i\|^2 \\ & + \mathbf{c}^\top \boldsymbol{\Sigma}_S \mathbf{c} - \mathbf{c}^\top \boldsymbol{\Sigma}_S (\boldsymbol{\Sigma}_S + \boldsymbol{\Sigma}_V)^{-1} \boldsymbol{\Sigma}_S^\top \mathbf{c}, \end{aligned} \quad (25a)$$

$$\text{subject to} \quad \|\boldsymbol{\alpha}_k\|^2 \leq \frac{P_k}{2}, \forall k \in [N_D], \quad (25b)$$

$$\frac{1}{2} \log \left(\frac{\det(\boldsymbol{\Sigma}_S + \boldsymbol{\Sigma}_V)}{\det(\boldsymbol{\Sigma}_V)} \right) \leq \sum_{i \in [N_A]} r_i, \quad (25c)$$

$$\frac{1}{2} \log \left(\frac{\det(\boldsymbol{\Sigma}_S + \boldsymbol{\Sigma}_V)}{\det([\boldsymbol{\Sigma}_S + \boldsymbol{\Sigma}_V]_{\mathcal{K}^c}) \det([\boldsymbol{\Sigma}_V]_{\mathcal{K}})} \right) \leq \sum_{i \in \mathcal{K}} r_i, \forall \mathcal{K} \subset [N_A], \mathcal{K} \neq \emptyset, \quad (25d)$$

where the power constraint in (25b) is from (8), the constraints (25c)-(25d) are from Lemma 1 and (16). To solve the optimization problem in (25), we propose an alternating optimization (AO) based algorithm, which is discussed in the following subsections.

B. Optimization of each $\boldsymbol{\alpha}$ with fixed $\boldsymbol{\beta}$, $\boldsymbol{\Sigma}_V$ and \mathbf{c}

With fixed $\{\boldsymbol{\alpha}_j\}_{j \neq k}$, $\{\boldsymbol{\beta}_i\}_{i=1}^{N_A}$, $\boldsymbol{\Sigma}_V$ and \mathbf{c} , the problem in (25) for optimizing $\boldsymbol{\alpha}_k$ reduces to

$$\begin{aligned} \underset{\boldsymbol{\alpha}_k}{\text{minimize}} \quad & \sum_{i_1 \in [N_A]} \sum_{i_2 \in [N_A]} [\boldsymbol{\Sigma}_S]_{i_1, i_2} \sum_{k \in \mathcal{N}_{D, i_1}} (\sqrt{v_k} - c_{i_1} \boldsymbol{\alpha}_k^\top \mathbf{H}_{i_1 k}^\top \boldsymbol{\beta}_{i_1}^\dagger)^H \\ & \times \sum_{k \in \mathcal{N}_{D, i_2}} (\sqrt{v_k} - c_{i_2} \boldsymbol{\alpha}_k^\top \mathbf{H}_{i_2 k}^\top \boldsymbol{\beta}_{i_2}^\dagger), \end{aligned} \quad (26a)$$

$$\text{subject to} \quad \|\boldsymbol{\alpha}_k\|^2 \leq \frac{P_k}{2}, \quad (26b)$$

where the objective function (26a) and the constraint (26b) are both convex w.r.t. $\boldsymbol{\alpha}_k$. Therefore, (26) is a convex quadratically constrained quadratic programming (QCQP) problem that can be solved using standard convex optimization tools.

C. Optimization of each β with fixed α , Σ_V and c

With fixed $\{\alpha_k\}_{k=1}^{N_D}$, $\{\beta_j\}_{j \neq i}$, Σ_V and c , the problem in (25) for optimizing β_i reduces to

$$\begin{aligned} \underset{\beta_i}{\text{minimize}} \quad & \sum_{i_1 \in [N_A]} \sum_{i_2 \in [N_A]} [\Sigma_S]_{i_1, i_2} \sum_{k \in \mathcal{N}_{D, i_1}} (\sqrt{v_k} - c_{i_1} \alpha_k^\top \mathbf{H}_{i_1 k}^\top \beta_{i_1}^\dagger)^\text{H} \\ & \times \sum_{k \in \mathcal{N}_{D, i_2}} (\sqrt{v_k} - c_{i_2} \alpha_k^\top \mathbf{H}_{i_2 k}^\top \beta_{i_2}^\dagger) + \varepsilon_i c_i^2 \|\beta_i\|^2. \end{aligned} \quad (27)$$

Since the problem in (27) is a quadratic convex problem, we set the derivative of (27) with respect to β_i to zero, yielding a closed-form expression of β_i^\dagger as

$$\beta_i^\dagger = \left(\varepsilon_i c_i \mathbf{I} + \sum_{j \in [N_A]} [\Sigma_S]_{i, j} \sum_{k \in \mathcal{N}_{D, i}} \mathbf{H}_{i k}^\dagger \alpha_k^\dagger \sum_{k \in \mathcal{N}_{D, j}} \alpha_k^\top \mathbf{H}_{j k}^\top \right)^{-1} \sum_{j \in [N_A]} [\Sigma_S]_{i, j} \sum_{k \in \mathcal{N}_{D, j}} \sqrt{v_k} \sum_{k \in \mathcal{N}_{D, i}} \mathbf{H}_{i k}^\dagger \alpha_k^\dagger, \quad (28)$$

which is used for updating β_i .

D. Optimization of c with fixed α , Σ_V and β

With fixed $\{\alpha_k\}_{k=1}^{N_D}$, $\{\beta_i\}_{i=1}^{N_A}$, Σ_V , the problem in (25) for optimizing c is converted into

$$\begin{aligned} \underset{c}{\text{minimize}} \quad & \sum_{i_1 \in [N_A]} \sum_{i_2 \in [N_A]} [\Sigma_S]_{i_1, i_2} \sum_{k \in \mathcal{N}_{D, i_1}} (\sqrt{v_k} - c_{i_1} \alpha_k^\top \mathbf{H}_{i_1 k}^\top \beta_{i_1}^\dagger)^\text{H} \\ & \times \sum_{k \in \mathcal{N}_{D, i_2}} (\sqrt{v_k} - c_{i_2} \alpha_k^\top \mathbf{H}_{i_2 k}^\top \beta_{i_2}^\dagger) + \sum_{i \in [N_A]} \varepsilon_i c_i^2 \|\beta_i\|^2 \\ & + c^\top [\Sigma_S - \Sigma_S (\Sigma_S + \Sigma_V)^{-1} \Sigma_S^\top] c, \end{aligned} \quad (29)$$

where $\Sigma_S - \Sigma_S (\Sigma_S + \Sigma_V)^{-1} \Sigma_S^\top$ is positive semidefinite. As the problem in (29) is a quadratic convex problem, we set the derivative of (29) with respect to c to zero, yielding

$$c = (\mathbf{T} + \mathbf{\Omega} + \Sigma_S - \Sigma_S (\Sigma_S + \Sigma_V)^{-1} \Sigma_S^\top)^{-1} \Sigma_S \begin{bmatrix} \text{Re}\{G_1\} \sum_{k \in \mathcal{N}_{D, 1}} \sqrt{v_k} \\ \vdots \\ \text{Re}\{G_{N_A}\} \sum_{k \in \mathcal{N}_{D, N_A}} \sqrt{v_k} \end{bmatrix} \quad (30)$$

where $\mathbf{\Omega} \triangleq \text{diag}(\varepsilon_1 \|\beta_1\|^2, \dots, \varepsilon_{N_A} \|\beta_{N_A}\|^2) \in \mathbb{R}^{N_A \times N_A}$ is a diagonal matrix, $\mathbf{T} \in \mathbb{R}^{N_A \times N_A}$ is a matrix with each entry $[\mathbf{T}]_{i, j} = [\Sigma]_{i, j} \text{Re}\{G_i^\dagger G_j\}$, and $G_i \triangleq \sum_{k \in \mathcal{N}_{D, i}} \alpha_k^\top \mathbf{H}_{i k}^\top \beta_i^\dagger \in \mathbb{C}$.

E. Optimization of Σ_V with fixed α , c and β

With fixed $\{\alpha_k\}_{k=1}^{N_D}$, $\{\beta_i\}_{i=1}^{N_A}$, c , the problem in (25) for optimizing Σ_V is reduced to

$$\text{maximize}_{\Sigma_V} \quad c^\top \Sigma_S (\Sigma_S + \Sigma_V)^{-1} \Sigma_S^\top c \quad (31a)$$

$$\text{subject to} \quad \frac{1}{2} \log \left(\frac{\det(\Sigma_S + \Sigma_V)}{\det(\Sigma_V)} \right) \leq \sum_{i \in [N_A]} r_i \quad (31b)$$

$$\frac{1}{2} \log \left(\frac{\det(\Sigma_S + \Sigma_V)}{\det([\Sigma_S + \Sigma_V]_{\mathcal{K}^c}) \det([\Sigma_V]_{\mathcal{K}})} \right) \leq \sum_{i \in \mathcal{K}} r_i, \forall \mathcal{K} \subset [N_A], \mathcal{K} \neq \emptyset. \quad (31c)$$

We solve the optimization problem in (31) through an iterative algorithm based on majorization-minimization (MM). The algorithm starts with a feasible point called the *current-point*. Each iteration round consists of two steps. In the first step, we construct a *surrogate* problem, whose objective serves as a lower bound of the original objective with equality holds at the current-point. Besides, the feasible region of the surrogate problem should be a subset of the original feasible region and contains the current-point. In the second step, we solve the surrogate problem, and the solution will be used as the current-point in the next iteration. Following [20], given a feasible point $\Sigma_V = \widehat{\Sigma}_V$, we provide a convex problem as the surrogate problem below

$$\text{maximize}_{\{\Sigma_V\}} \quad 2c^\top \Sigma_S b - b^\top (\Sigma_S + \Sigma_V) b \quad (32a)$$

$$\text{s.t.} \quad \chi_{\mathcal{K}}(\mathbf{E}_{\mathcal{K}}, \mathbf{F}_{\mathcal{K}}, \Sigma_V) + \xi_{\mathcal{K}}(\mathbf{E}_{\mathcal{K}}, \mathbf{F}_{\mathcal{K}}) \leq \sum_{i \in \mathcal{K}} r_i, \forall \mathcal{K} \subset [N_A], \mathcal{K} \neq \emptyset, \quad (32b)$$

$$\chi_{[N_A]}(\mathbf{G}, \Sigma_V) + \xi_{[N_A]}(\mathbf{G}) \leq \sum_{i \in [N_A]} r_i, \quad (32c)$$

where

$$\chi_{\mathcal{K}}(\mathbf{E}_{\mathcal{K}}, \mathbf{F}_{\mathcal{K}}, \Sigma_V) = \frac{\log(e)}{2} \text{tr} \{ \mathbf{F}_{\mathcal{K}}^{-1} [\Sigma_V]_{\mathcal{K}} \} + \frac{\log(e)}{2} \text{tr} \{ \mathbf{E}_{\mathcal{K}}^\top \mathbf{F}_{\mathcal{K}}^{-1} \mathbf{E}_{\mathcal{K}} [\Sigma_V]_{\mathcal{K}^c} \} - \frac{1}{2} \log(\det([\Sigma_V]_{\mathcal{K}})), \quad (33a)$$

$$\begin{aligned} \xi_{\mathcal{K}}(\mathbf{E}_{\mathcal{K}}, \mathbf{F}_{\mathcal{K}}) &= \frac{\log(e)}{2} \text{tr} \{ \mathbf{F}_{\mathcal{K}}^{-1} ([\Sigma_S]_{\mathcal{K}} + \mathbf{E}_{\mathcal{K}} [\Sigma_S]_{\mathcal{K}^c} \mathbf{E}_{\mathcal{K}}^\top - \mathbf{E}_{\mathcal{K}} [\Sigma_S]_{\mathcal{K}^c, \mathcal{K}} - [\Sigma_S]_{\mathcal{K}, \mathcal{K}^c} \mathbf{E}_{\mathcal{K}}^\top) \} \\ &\quad + \frac{1}{2} \log(\det(\mathbf{F}_{\mathcal{K}})) - \frac{|\mathcal{K}| \log(e)}{2}, \end{aligned} \quad (33b)$$

$$\chi_{[N_A]}(\mathbf{G}, \Sigma_V) = \frac{\log(e)}{2} \text{tr} \{ \mathbf{G}^{-1} \Sigma_V \} - \frac{1}{2} \log(\det(\Sigma_V)), \quad (33c)$$

$$\xi_{[N_A]}(\mathbf{G}) = \frac{1}{2} \log(\det(\mathbf{G})) + \frac{\log(e)}{2} \text{tr} \{ \mathbf{G}^{-1} \Sigma_X \} - \frac{N_A \log(e)}{2}, \quad (33d)$$

and $\mathbf{b} = (\boldsymbol{\Sigma}_S + \widehat{\boldsymbol{\Sigma}}_V)^{-1} \boldsymbol{\Sigma}_S \mathbf{c}$, $\mathbf{G} = \boldsymbol{\Sigma}_S + \widehat{\boldsymbol{\Sigma}}_V$, $\mathbf{E}_{\mathcal{K}} = [\boldsymbol{\Sigma}_S]_{\mathcal{K}, \mathcal{K}^c} ([\boldsymbol{\Sigma}_S + \widehat{\boldsymbol{\Sigma}}_V]_{\mathcal{K}^c})^{-1}$, and $\mathbf{F}_{\mathcal{K}} = [\boldsymbol{\Sigma}_S + \widehat{\boldsymbol{\Sigma}}_V]_{\mathcal{K}} - [\boldsymbol{\Sigma}_S]_{\mathcal{K}, \mathcal{K}^c} ([\boldsymbol{\Sigma}_S + \widehat{\boldsymbol{\Sigma}}_V]_{\mathcal{K}^c})^{-1} [\boldsymbol{\Sigma}_S]_{\mathcal{K}^c, \mathcal{K}}$ for all nonempty set $\mathcal{K} \subset [N_A]$. Since the surrogate problem (32) is convex and is solved optimally with existing convex optimization solvers such as CVXPY [23]. By repeatedly constructing and solving this surrogate problem following the MM framework introduced before, we finally obtain a suboptimal solution to the original problem (31). The overall optimization process is outlined in Algorithm 2.

Algorithm 2 The Overall Optimization Process.

- 1: Each device k computes v_k, P_k and sends them to AP i , if $k \in \mathcal{N}_{D,i}$
 - 2: Each AP i receives $\{v_k, P_k\}_{k \in \mathcal{N}_{D,i}}$ from the devices and sends them to the CS
 - 3: Each AP i estimates $\{\mathbf{H}_{ik}\}_{k \in \mathcal{N}_{D,i}}, \varepsilon_i$ and sends them to the CS
 - 4: The CS receives $\{\{\mathbf{H}_{ik}\}_{k \in \mathcal{N}_{D,i}}, \varepsilon_i, \{v_k, P_k\}_{k \in \mathcal{N}_{D,i}}\}_{i=1}^{N_A}$ from the APs
 - 5: The CS estimates $\boldsymbol{\Sigma}_S$
 - 6: **repeat**
 - 7: The CS optimizes $\{\boldsymbol{\alpha}_k\}_{k=1}^{N_D}$ via solving the problem in (26)
 - 8: The CS optimizes $\{\boldsymbol{\beta}_i\}_{i=1}^{N_A}$ via (27)
 - 9: The CS optimizes $\boldsymbol{\Sigma}_V$ via iteratively solving the surrogate problem in (31)
 - 10: The CS optimizes \mathbf{c} via (29)
 - 11: **until** convergence
 - 12: The CS sends $\{\boldsymbol{\alpha}_k\}_{k \in \mathcal{N}_{D,i}}, \boldsymbol{\beta}_i$ to each AP i
 - 13: Each AP i sends $\boldsymbol{\alpha}_k$ to the device k , if $k \in \mathcal{N}_{D,i}$
-

VI. PRACTICAL DESIGN

In this section, we provide a practical design of encoding functions $\{f_i^{(t)}\}_{i=1}^{N_A}$ and joint decoding function $f^{(t)}$. In this design, we consider a quadratic distortion measure $d(\mathbf{a}^{(t)}, \mathbf{b}^{(t)}) = \|\mathbf{a}^{(t)} - \mathbf{b}^{(t)}\|^2$ and the linear aggregation target $\kappa(\mathbf{a}_1^{(t)}, \dots, \mathbf{a}_{N_A}^{(t)}) = \sum_{i=1}^{N_A} c_i^{(t)} \mathbf{a}_i^{(t)}$.

A. Encoding Function Design

As shown in Fig. 3, we propose an encoding function $f_i^{(t)}, \forall i$ that comprises a compression module, quantization module and error accumulation module. Specifically, at the t -th round, the source vector $\mathbf{s}_i^{(t)}$ is firstly compressed into a low-dimensional vector as

$$\hat{\mathbf{s}}_i^{(t)} = \mathbf{A} \mathbf{s}_i^{(t)} \in \mathbb{R}^{N_\sigma}, \forall i \in [N_A], \quad (34)$$

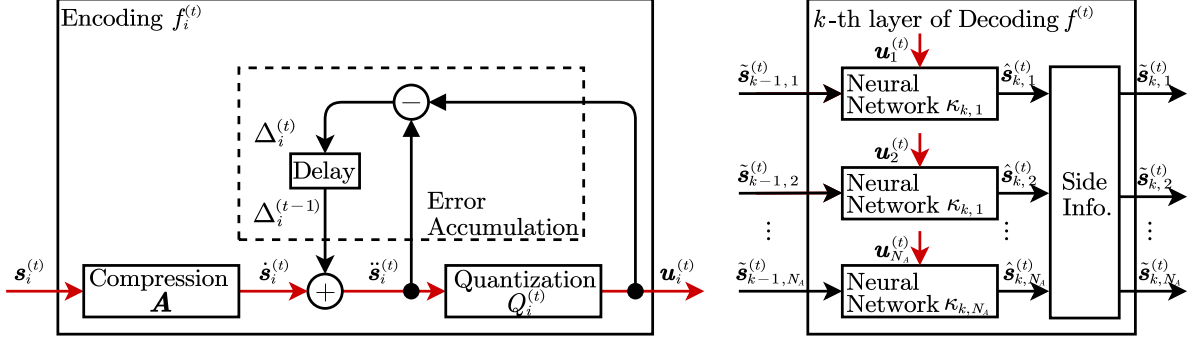


Fig. 3. An illustration of the encoding function $f_i^{(t)}$, $\forall i$ and layer k on decoding function $f^{(t)}$.

where $\mathbf{A} \in \mathbb{R}^{N\sigma \times N}$ is a random compression matrix with a compression ratio of $\sigma \in (0, 1]$. To reduce quantization error from the previous round, $\hat{\mathbf{s}}_i^{(t)}$ is added with an error accumulation term [24] as

$$\ddot{\mathbf{s}}_i^{(t)} = \hat{\mathbf{s}}_i^{(t)} + \Delta_i^{(t-1)} \in \mathbb{R}^{N\sigma}, \forall i \in [N_A], \quad (35)$$

where the error accumulation term $\Delta_i^{(t-1)} \in \mathbb{R}^{N\sigma}$ is from the round $t-1$. To meet the rate-constraint in Definition 1 and (16), i.e., $\frac{1}{N} \log(B_i^{(t)}) \leq r_i^{(t)} + \epsilon$, $\forall i \in [N_A]$, the resulting vector $\ddot{\mathbf{s}}_i^{(t)}$ is next quantized to

$$\mathbf{u}_i^{(t)} = \mathcal{Q}_i^{(t)}(\ddot{\mathbf{s}}_i^{(t)}, r_i^{(t)}) \in [B_i^{(t)}], \forall i \in [N_A], \quad (36)$$

where $B_i^{(t)}$ given in (11) is the codebook size of encoding function $f_i^{(t)}$, $\mathcal{Q}_i^{(t)}$ is an A-law quantizer that discretizes each element of $\ddot{\mathbf{s}}_i^{(t)}$ into a quantized number, resulting in vector $\mathbf{u}_i^{(t)}$. The error accumulation vector $\Delta_i^{(t)}$ is calculated as

$$\Delta_i^{(t)} = \ddot{\mathbf{s}}_i^{(t)} - \mathbf{u}_i^{(t)} \in \mathbb{R}^{N\sigma}, \forall i \in [N_A]. \quad (37)$$

Finally, each AP i sends the quantized vector $\mathbf{u}_i^{(t)}$ to the CS through the uplink fronthaul network.

B. Decoding Function Design

As shown in Fig. 3, we propose a decoding function $f^{(t)}$ with K layers, each consisting of N_A neural networks and a side information module. At layer k , each neural network $\kappa_{k,i}^{(t)}(\cdot)$, $\forall i$ computes

$$\hat{\mathbf{s}}_{k,i}^{(t)} = \kappa_{k,i}^{(t)}(\mathbf{u}_i^{(t)}, \tilde{\mathbf{s}}_{k-1,i}^{(t)}) \in \mathbb{R}^N, \forall i \in [N_A], \quad (38)$$

Algorithm 3 Practical Design of Encoding and Decoding Functions.

1: **Each encoding function** $f_i^{(t)}$ **in (11) does:**

2: Compute $\mathbf{u}_i^{(t)}$ via (34)-(36)

3: Compute $\Delta_i^{(t)}$ via (37)

4: **The decoding function** $f^{(t)}$ **in (12) does:**

5: Initialize $\tilde{\mathbf{s}}_{0,i}^{(t)} = \mathbf{0}, \forall i$

6: **for** $k = 1, \dots, K$:

7: Compute $\{\hat{\mathbf{s}}_{k,i}^{(t)}, \tilde{\mathbf{s}}_{k,i}^{(t)}\}_{i=1}^{N_A}$ via (38)-(39)

8: **end**

9: Compute $\hat{\mathbf{z}}^{(t)}$ via (40)

10: **The training process w.r.t.** $\mathbf{w}^{(t)}$:

11: Initialize $\tilde{\mathbf{s}}_{0,i}^{(t)} = \mathbf{0}, \forall i, t$

12: **repeat**

13: Sample data $\mathbf{s}_1^{(t)}, \dots, \mathbf{s}_{N_A}^{(t)}$ from a memoryless Gaussian source $\mathcal{N}(\mathbf{0}, \Sigma_S^{(t)})$

14: Compute the loss in (41)

15: Update $\mathbf{w}^{(t)}$ through backpropagation

16: **until** convergence

where $\mathbf{u}_i^{(t)}$ is the encoded vector from AP i , and $\tilde{\mathbf{s}}_{i,k-1}^{(t)} \in \mathbb{R}^N, \forall i$ is a side information module from layer $k-1$, with $\tilde{\mathbf{s}}_{i,0}^{(t)}$ initialized to $\mathbf{0}$. Then the side information module at layer k collects $\{\hat{\mathbf{s}}_{k,i}^{(t)}\}_{i=1}^{N_A}$ to generate the side information vector as

$$\tilde{\mathbf{s}}_{k,i}^{(t)} = \sum_{j \in [N_A], j \neq i} \hat{\mathbf{s}}_{k,j}^{(t)} \in \mathbb{R}^N, \forall i \in [N_A]. \quad (39)$$

Considered a linear aggregation target, i.e., $\kappa(\mathbf{a}_1^{(t)}, \dots, \mathbf{a}_{N_A}^{(t)}) = \sum_{i=1}^{N_A} c_i^{(t)} \mathbf{a}_i^{(t)}$, the encoding function $f^{(t)}$ constructs the estimation $\hat{\mathbf{z}}^{(t)}$ as

$$\hat{\mathbf{z}}^{(t)} = \sum_{i=1}^{N_A} c_i^{(t)} \mathbf{s}_{K,i}^{(t)}, \quad (40)$$

where $\mathbf{s}_{K,i}^{(t)}$ is the vector from layer K . To train the neural networks in $f^{(t)}$ at each round t , based on the quadratic distortion measure and the linear aggregation target, we design an empirical

objective as

$$\underset{\mathbf{w}^{(t)}}{\text{maximize}} \left\| \mathbf{z}^{(t)} - \hat{\mathbf{z}}^{(t)} \right\|^2 \triangleq \left\| \sum_{i \in [N_A]} c_i^{(t)} \mathbf{s}_i^{(t)} - f^{(t)}(\mathbf{u}_1^{(t)}, \dots, \mathbf{u}_{N_A}^{(t)}, \mathbf{w}^{(t)}) \right\|^2, \quad (41)$$

where $\mathbf{u}_i^{(t)} = f_i^{(t)}(\mathbf{s}_i^{(t)})$, $\mathbf{w} \in \mathbb{R}^M$ is the network parameter of decoding $f^{(t)}$ with dimension M , and $s_{1,n}^{(t)}, \dots, s_{N_A,n}^{(t)}, \forall n$ are sampled from a memoryless Gaussian source $\mathcal{N}(\mathbf{0}, \Sigma_S^{(t)})$. The minimization of (41) is through the gradient descent (GD) w.r.t. \mathbf{w} . The overall design of encoding functions and decoding function is summarized in Algorithm 3.

C. Optimization in Practical Design

In practical encoding and decoding function designs, $\Sigma_V^{(t)}$ is not an optimization variable. Therefore, the optimization of practical design is similar to the problem in (25) but does treat $\Sigma_V^{(t)}$ as a known constant. To estimate $\Sigma_V^{(t)}$, we follow [20], to set the compression ratio $\sigma = 1$ for each AP and define the i -th diagonal element of $\Sigma_V^{(t)}$ as $\frac{1}{N}(\mathbf{s}_i^{(t)} - \mathbf{u}_i^{(t)})^\top (\mathbf{s}_i^{(t)} - \mathbf{u}_i^{(t)})$. In practice, we require each AP to send a sub-vector of $\mathbf{s}_i - \mathbf{u}_i^{(t)}$ to the CS intermittently for estimation during training.

VII. NUMERICAL RESULTS

A. Experimental Settings

We validate our proposed OA-FL in MIMO Cloud-RAN framework with experiments, and provide some schemes for comparison:

- Error-free bound: This bound assumes that the CS receives all the local updates of devices in an error-free fashion and updates the global model by (3).
- L-DSC bound: In our proposed OA-FL in MIMO Cloud-RAN framework, this bound considers L-DSC encoding at each AP and L-DSC decoding at the CS [20]. We emphasize that the L-DSC encoding and decoding serve as a benchmark for theoretical performance limit.
- Proposed practical design: In our proposed OA-FL in MIMO Cloud-RAN framework, this scheme uses the practical design proposed in Section VI as the encoding and decoding functions.
- Quantization: In our proposed OA-FL in MIMO Cloud-RAN framework, this scheme is applied as follows: each AP i computes the encoded vector $\mathbf{u}_i^{(t)}$ as $\mathbf{u}_i^{(t)} = \mathcal{Q}_i^{(t)}(\mathbf{s}_i^{(t)}, r_i^{(t)})$, $\forall t, i$, and the CS computes the global update $\hat{\mathbf{z}}^{(t)}$ as $\hat{\mathbf{z}}^{(t)} = \sum_{i=1}^{N_A} c_i^{(t)} \mathbf{u}_i^{(t)} \in \mathbb{R}^N, \forall t$.

TABLE I
SIMULATION SETTINGS

Parameter	Value	Parameter	Value	Parameter	Value	Parameter	Value	Parameter	Value
N_T	3	N_R	8	α	3.8	ν	-60 dB	δ_{ik}	30 m
$G_{R,i}$	10 dBi	$G_{T,k}$	5 dBi	P_k	1 W	σ_z^2	-80 dBm	σ	0.5

- **Distributed deterministic information bottleneck (DDIB):** In our proposed OA-FL in MIMO Cloud-RAN framework, this scheme considers DDIB encoding at each AP and DDIB decoding at the CS, both of which are based on deep neural networks (DNN).

To make performance comparisons, we conduct federated image classification experiments on three datasets: the MNIST dataset of handwritten digits [25], the Fashion-MNIST dataset of fashion clothing [26] and the CIFAR-10 dataset. We train a neural network on each device and the CS with two 5×5 convolution layers (the first with 10 channels, the second with 20, each followed by a 2×2 max pooling operation), a fully connected layer with 50 units and ReLU activation, and a final softmax output layer (model parameter length $N = 21840$). Each device performs 5 stochastic gradient descent updates with a learning rate of 0.01 and a local batch size of 1200. The CS updates the global model using a learning rate of $1.5/(1+t/10)$, where t is the communication round. The channel gain is modeled according to [27], where the channel gain is given by $\mathbf{H}_{ik}^{(t)} = \sqrt{G_{R,i}G_{T,k}\nu\delta_{ik}^{-\alpha}}\tilde{\mathbf{H}}_{ik}^{(t)}$. Here, the entries of $\tilde{\mathbf{H}}_{ik}^{(t)}$ are modeled as i.i.d. circularly symmetric complex Gaussian random variables with zero-mean and unit-variance, $G_{R,i}$ and $G_{T,k}$ are the antenna gains at AP i and device k , respectively, α is the path loss exponent, δ_{ik} is the distance between device k and AP i , and ν is the path loss at a reference distance of 1 m [28]. We summarize the simulation settings in Tab. I.

B. Comparisons of the Proposed Algorithms Under Various Settings

To verify the effectiveness of side information module in the proposed practical design, we present a comparison method called "Proposed practical design (zero side information)", where the side information vector $\tilde{\mathbf{s}}_{k,i}^{(t)}, \forall k, i, t$ is set to $\mathbf{0}$. Fig. 4 shows the performance of our proposed practical design in utilizing the inter-AP correlation. The left of Fig. 4 shows the training loss of the proposed practical design, i.e., the objective in (41). The middle of Fig. 4 shows the system mean square error (MSE), i.e. $\|\mathbf{e}\|^2$ versus round t . We observe that the proposed practical design achieves lower training loss and MSE than the proposed practical design (zero side information),

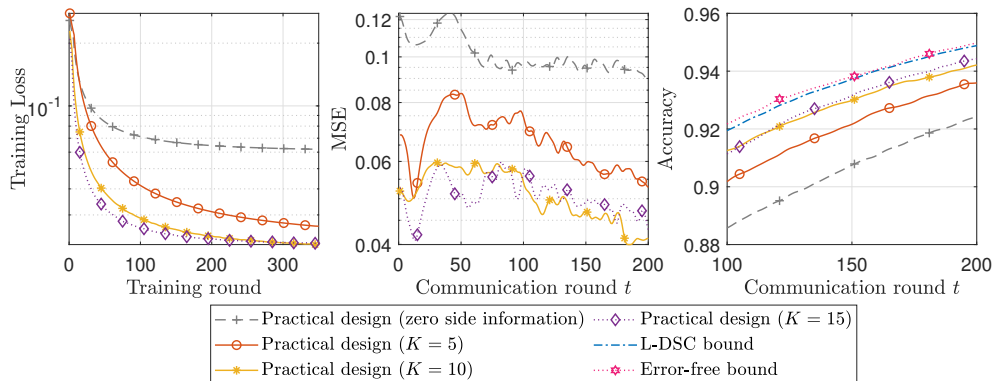


Fig. 4. **Left:** Training loss of the proposed practical design, i.e., the objective in (41). **Middle:** The system mean square error on MNIST dataset, i.e. $\|e\|^2$ versus round t . **Right:** The test accuracy on MNIST dataset versus round t . Other setting: $N_A = 3, \mathcal{N}_{D,1} = 1, \dots, 5, \mathcal{N}_{D,2} = 6, \dots, 13, \mathcal{N}_{D,3} = 14, \dots, 20, r_i^{(t)} = 1$ bit/symbol, $\forall i, t, K = 10$.

thanks to the ability of the side information module to leverage inter-AP correlation. Moreover, as we increased the number of layers K , we see a decrease in both the training loss and system MSE. This improvement comes at the expense of increased computational complexity and latency, which is a reasonable trade-off. The right of Fig. 4 shows the test accuracy on MNIST dataset versus round t . We see that by utilizing the side information module, the test accuracy of the proposed practical design was close to the L-DSC bound and the error-free bound, with a deviation of less than 1% at convergence. Additionally, the proposed practical design significantly outperformed the proposed practical design (zero side information), which further demonstrates the advantage of leveraging the inter-AP correlation.

To demonstrate the effectiveness of the optimization process in Algorithm 2, we designed three scenarios, which are depicted in the left, middle, and right sections of Fig. 5. In the first scenario, all devices have the same transmission power, and all APs have the same information rate limitation, e.g., $P_k^{(t)} = 1W, \forall k, t, \tilde{r}_i^{(t)} = 10$ bit/symbol, $\forall i, t$. In the second scenario, devices have varying transmission power and APs have differing information rate limitations, e.g., $P_k^{(t)} = 0.5W, \forall k \in \mathcal{N}_{D,1}, P_k^{(t)} = 1W \forall k \in \mathcal{N}_{D,2} \cup \mathcal{N}_{D,3}, r_1^{(t)} = 2$ bit/symbol, $r_2^{(t)} = r_3^{(t)} = 10$ bit/symbol. In the third scenario, we follow a similar settings as in the first scenario, but with reduced transmission power for all devices and lowered information rate limitation for all APs, e.g., $P_k^{(t)} = 0.5W, \forall k, t, r_i^{(t)} = 2$ bit/symbol, $\forall i, t$. We also included two comparison methods, "Proposed practical design (without optimized c)" and "L-DSC bound (without optimized c)". In these

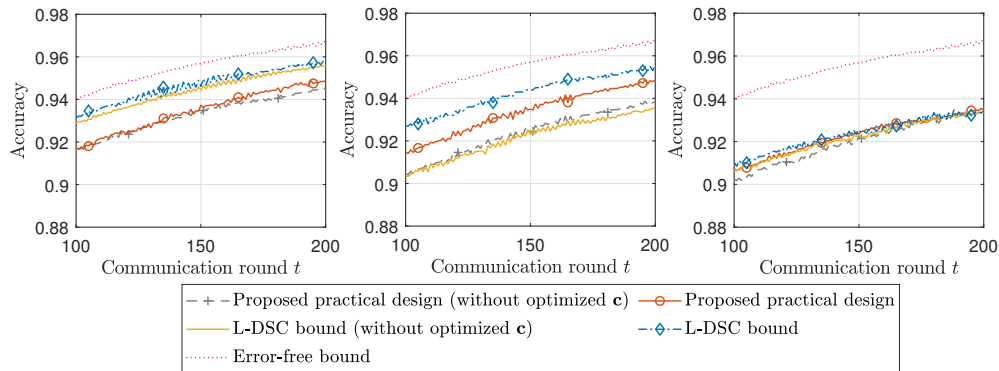


Fig. 5. The curves show the test accuracy and mean-square error (MSE) on the MNIST dataset versus training round t . The settings are as follows: $N_A = 3$, $\mathcal{N}_{D,1} = 1, \dots, 5$, $\mathcal{N}_{D,2} = 6, \dots, 13$, and $\mathcal{N}_{D,3} = 14, \dots, 20$. **Left:** $P_k^{(t)} = 1\text{W}$, $\forall k, t$, $r_i^{(t)} = 10$ bit/symbol, $\forall i, t$. **Middle:** $P_k^{(t)} = 0.5\text{W}$, $\forall k \in \mathcal{N}_{D,1}$, $P_k^{(t)} = 1\text{W}$ $\forall k \in \mathcal{N}_{D,2} \cup \mathcal{N}_{D,3}$. $r_1^{(t)} = 2$ bit/symbol, $r_2^{(t)} = r_3^{(t)} = 10$ bit/symbol. **Right:** $P_k^{(t)} = 0.5\text{W}$, $\forall k, t$, $r_i^{(t)} = 2$ bit/symbol, $\forall i, t$, $K = 10$.

methods, the weighted parameter is fixed at $c = 1$. Fig. 5 shows that optimizing c results in a small improvement in performance in the left and right plots, but a significant improvement in the middle plot. Specifically, in the middle plot, the L-DSC bound achieves an accuracy improvement of approximately 0.017 at the convergence point, while the proposed practical design achieves an improvement of approximately 0.011. These results suggest that optimizing c enhance the learning performance when the communication quality across different APs is unbalanced, as in scenario (2). By examining the optimization problem of c in (29), we see that the optimization of c is actually a resource allocator that measures the wired communication quality of different APs to the CS and the wireless communication quality of different APs to their respective served devices. Additionally, we noted that in scenarios where the channel environment is degraded, i.e., the right plot, the test accuracy of the proposed practical design is comparable to the L-DSC bound.

To demonstrate the performance of the proposed practical design in various rate constraints, we provide Fig. 6. In this figure, we present three different rate constraint settings, as denoted by $\tilde{r}_i^{(t)}$, which determine the maximum number of bits that AP i can transmit to the CS during each training round t . The left and middle of Fig. 4 show the training loss and MSE of proposed practical design under various rate constraints. We see that the training loss and MSE of the proposed practical design exhibit a significant increase when the rate constraint, i.e., $\tilde{r}_i^{(t)}$, is close to the data dimension N , compared to when it is close to $2N$ or $4N$. The right of Fig.

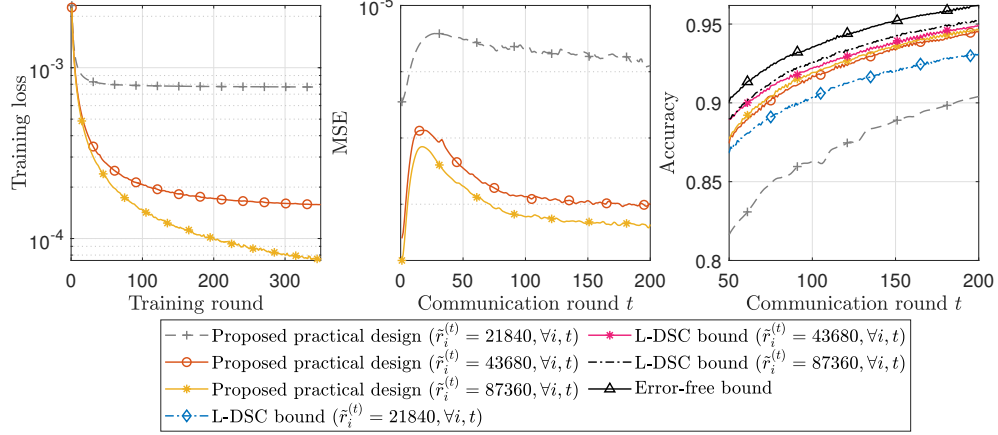


Fig. 6. **Left:** Training loss of the proposed practical design, i.e., the objective in (41). **Middle:** The system mean square error on MNIST dataset, i.e. $\|e\|^2$ versus training round t . **Right:** The test accuracy on MNIST dataset versus training round t . Other setting: $N_A = 3, \mathcal{N}_{D,1} = 1, \dots, 5, \mathcal{N}_{D,2} = 6, \dots, 13, \mathcal{N}_{D,3} = 14, \dots, 20, K = 10$.

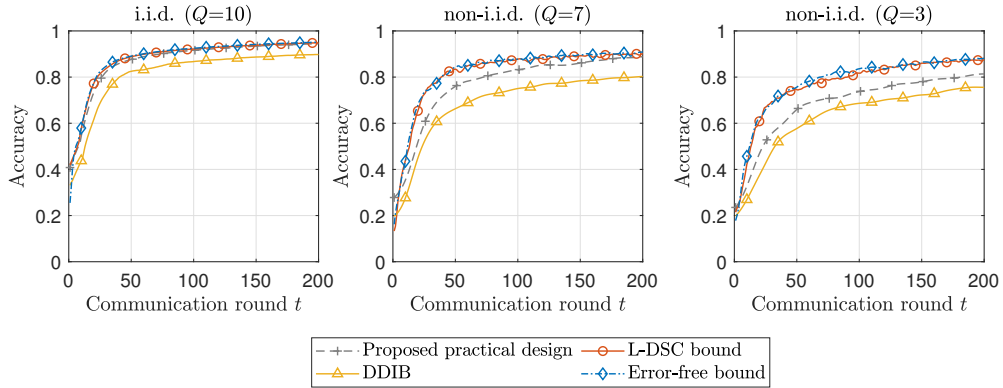


Fig. 7. Test accuracy on the MNIST task, where Q measures the heterogeneous setting to a certain extent. **Left:** Independent and identically distributed (i.i.d.) dataset with $Q = 10$. **Middle:** non-i.i.d. dataset with $Q = 7$. **Right:** non-i.i.d. dataset with $Q = 3$. Other setting: $N_A = 3, \mathcal{N}_{D,1} = 1, \dots, 5, \mathcal{N}_{D,2} = 6, \dots, 13, \mathcal{N}_{D,3} = 14, \dots, 20, K = 10$.

6 compares the test accuracy of our practical design with the L-DSC bound and the error-free bound. At convergence, the accuracy of our practical design is within 0.01 of the L-DSC bound when $\tilde{r}_i^{(t)}$ is equal to $4N$ or $2N$, and within 0.025 when $\tilde{r}_i^{(t)}$ is equal to N .

C. Comparisons With Existing Schemes

We empirically validate the heterogeneous setting of federated datasets in our framework using the MNIST task. Specifically, each device randomly selects Q classes from the dataset $\{\mathcal{B}_k\}_{k=1}^{N_D}$,

and subsequently samples are randomly drawn without repetition from these selected classes. When Q is set to 10, the local datasets of the devices are independently and identically distributed (i.i.d.). Fig. 7 compares the test accuracy between proposed practical design and other baseline schemes under different heterogeneous settings. We observe that as the value of Q decreases, the learning performance of these schemes also decreases. We also see that the proposed practical design achieves a learning performance comparable to the L-DSC bound at the convergence point when Q is set to either 10 or 7. Furthermore, the proposed practical design outperforms the quantization scheme and the DDIB scheme across all heterogeneous settings.

VIII. CONCLUSIONS

In this paper, we proposed the OA-FL in MIMO Cloud-RAN framework to address the issues of limited server coverage and low resource utilization in traditional OA-FL. We also noted that inter-AP correlation can be leveraged to improve learning performance and therefore proposed modeling the global aggregation stage as an L-DSC problem to make analysis from the perspective of rate-distortion theory. We further analyzed the performance of the proposed OA-FL in MIMO Cloud-RAN framework. Based on this analysis, we formulated a communication-learning optimization problem to improve the system performance by considering the inter-AP correlation. We showed that, under mild conditions, the problem can be solved using alternating optimization (AO) and majorization-minimization (MM). Subsequently, we proposed a practical design that demonstrates the utilization of inter-AP correlation. The numerical results show that the proposed practical design effectively leverages inter-AP correlation, and outperforms other baseline schemes.

APPENDIX A

SYSTEM ERROR BOUND

To start with, we bound $\mathbb{E}[\|e^{(t)}\|^2]$ as

$$\mathbb{E}[\|e^{(t)}\|^2] \leq 2(\mathbb{E}[\|e_1^{(t)}\|^2] + \mathbb{E}[\|e_2^{(t)}\|^2]), \quad (42)$$

by using the triangle inequality and the inequality of arithmetic means. With (6), (9)-(10), (18), we have

$$\mathbb{E}[\|e_1^{(t)}\|^2] = \mathbb{E} \left[\left\| \sum_{i \in [N_A]} \sum_{k \in \mathcal{N}_{D,i}} \left(\sqrt{v_k^{(t)}} - c_i^{(t)} \boldsymbol{\alpha}_k^{(t)\top} \mathbf{H}_{ik}^{(t)\top} \boldsymbol{\beta}_i^{(t)\dagger} \right) \mathbf{r}_k^{(t)} - \sum_{i \in [N_A]} c_i^{(t)} \mathbf{z}_i^{(t)\top} \boldsymbol{\beta}_i^{(t)\dagger} \right\|^2 \right]. \quad (43)$$

Since the term $\mathbf{Z}_i, \forall i \in [N_A]$ is an independent Gaussian random matrix, we have

$$\mathbb{E}[\|\mathbf{e}_1^{(t)}\|^2] \leq \mathbb{E} \left[\left\| \sum_{i \in [N_A]} \sum_{k \in \mathcal{N}_{D,i}} \left(\sqrt{v_k^{(t)}} - c_i^{(t)} \boldsymbol{\alpha}_k^{(t)\top} \mathbf{H}_{ik}^{(t)\top} \boldsymbol{\beta}_i^{(t)\dagger} \right) \mathbf{r}_k^{(t)} \right\|^2 \right] + \sum_{i \in [N_A]} \mathbb{E} \left[\left\| c_i^{(t)} \mathbf{Z}_i^{(t)\top} \boldsymbol{\beta}_i^{(t)\dagger} \right\|^2 \right]. \quad (44)$$

From the assumption in Lemma 2, we have

$$\begin{aligned} \mathbb{E}[\|\mathbf{e}_1^{(t)}\|^2] &\leq N \sum_{i_1 \in [N_A]} \sum_{i_2 \in [N_A]} [\boldsymbol{\Sigma}_{\mathbf{S}}^{(t)}]_{i_1, i_2} \sum_{k \in \mathcal{N}_{D, i_1}} \left(\sqrt{v_k^{(t)}} - c_{i_1}^{(t)} \boldsymbol{\alpha}_k^{(t)\top} \mathbf{H}_{i_1 k}^{(t)\top} \boldsymbol{\beta}_{i_1}^{(t)\dagger} \right)^H \\ &\quad \times \sum_{k \in \mathcal{N}_{D, i_2}} \left(\sqrt{v_k^{(t)}} - c_{i_2}^{(t)} \boldsymbol{\alpha}_k^{(t)\top} \mathbf{H}_{i_2 k}^{(t)\top} \boldsymbol{\beta}_{i_2}^{(t)\dagger} \right) + N \sum_{i \in [N_A]} \varepsilon_i^{(t)} c_i^{(t)2} \|\boldsymbol{\beta}_i^{(t)}\|^2, \end{aligned} \quad (45)$$

where $\varepsilon_i \triangleq \frac{1}{N} \mathbb{E}[\|\mathbf{Z}_i^{(t)}\|^2] \in \mathbb{R}, \forall i \in [N_A]$. The closed-form expressions of the terms $\mathbb{E}[\|\mathbf{e}_1^{(t)}\|^2] = \frac{1}{N} \mathbb{E}[\|\mathbf{z}^{(t)} - \hat{\mathbf{z}}^{(t)}\|^2]$ is given in Lemma 1. From (42), (45) and Lemma 1, we have the closed-form bound of $\mathbb{E}[\|\mathbf{e}^{(t)}\|^2]$ in (19), which completes the proof.

REFERENCES

- [1] K. He, X. Zhang, S. Ren, and J. Sun, "Deep residual learning for image recognition," in *Proc. IEEE Comput. Soc. Conf. Comput. Vision Pattern Recognit.*, Las Vegas, NV, USA, 2016, pp. 770–778.
- [2] T. Young, D. Hazarika, S. Poria, and E. Cambria, "Recent trends in deep learning based natural language processing," *IEEE Computat. Intell. Mag.*, vol. 13, no. 3, pp. 55–75, 2018.
- [3] J. Goetz, K. Malik, D. Bui, S. Moon, H. Liu, and A. Kumar, "Active federated learning," *arXiv preprint arXiv:1909.12641*, 2019.
- [4] E. b. P. Kairouz and H. B. McMahan, "Advances and open problems in federated learning," *MAL*, vol. 14, no. 1, 2021.
- [5] B. Nazer and M. Gastpar, "Computation over multiple-access channels," *IEEE Trans. Inf. Theory*, vol. 53, no. 10, pp. 3498–3516, 2007.
- [6] G. Zhu, Y. Du, D. Gunduz, and K. Huang, "One-bit over-the-air aggregation for communication-efficient federated edge learning," *IEEE Trans. Wireless Commun.*, vol. 20, no. 3, pp. 2120–2135, 2021.
- [7] D. Wen, G. Zhu, and K. Huang, "Reduced-dimension design of MIMO over-the-air computing for data aggregation in clustered IoT networks," *IEEE Trans. Wirel. Commun.*, vol. 18, no. 11, pp. 5255–5268, 2019.
- [8] K. Chen and R. Duan, "China mobile research institute, C-RAN the road towards green RAN, White paper, v2.5," 2013. [Online]. Available: https://web.archive.org/web/20131231095559/http://labs.chinamobile.com/cran/wp-content/uploads/CRAN_white_paper_v2_5_EN.pdf
- [9] F. Richter, A. J. Fehske, and G. P. Fettweis, "Energy efficiency aspects of base station deployment strategies for cellular networks," in *2009 IEEE 70th Vehicular Technology Conference Fall*, Anchorage, Alaska, USA, 2009, pp. 1–5.
- [10] S.-H. Park, O. Simeone, O. Sahin, and S. Shamai Shitz, "Fronthaul compression for cloud radio access networks: Signal processing advances inspired by network information theory," *IEEE Signal Proc. Mag.*, vol. 31, no. 6, pp. 69–79, 2014.
- [11] D. Pompili, A. Hajisami, and H. Viswanathan, "Dynamic provisioning and allocation in cloud radio access networks (C-RANs)," *Ad Hoc. Netw.*, vol. 30, pp. 128–143, 2015.

- [12] C. Zhong, H. Yang, and X. Yuan, "Over-the-air multi-task federated learning over MIMO interference channel," *arXiv preprint arXiv:2112.13603*, 2021.
- [13] A. Checko, H. L. Christiansen, Y. Yan, L. Scolari, G. Kardaras, M. S. Berger, and L. Dittmann, "Cloud RAN for mobile networks: A technology overview," *IEEE Comms. Surv. Tut.*, vol. 17, no. 1, pp. 405–426, 2015.
- [14] O. Abari, H. Rahul, and D. Katabi, "Over-the-air function computation in sensor networks," *arXiv preprint arXiv:1612.02307*, 2016.
- [15] J. Dong, Y. Shi, and Z. Ding, "Blind over-the-air computation and data fusion via provable Wirtinger flow," *IEEE Trans. Signal Process.*, vol. 68, pp. 1136–1151, 2020.
- [16] "3GPP specifications." Sep. 2010. [Online]. Available: <http://4g5gworld.com/blog/timing-advance-ta-lte>
- [17] H. Liu, X. Yuan, and Y.-J. A. Zhang, "Reconfigurable intelligent surface enabled federated learning: A unified communication-learning design approach," *arXiv preprint arXiv:2011.10282*, 2021.
- [18] M. Amiri and D. Gündüz, "Federated learning over wireless fading channels," *IEEE Trans. Wirel. Commun.*, vol. 19, no. 5, pp. 3546–3557, 2020.
- [19] D. Yu, S.-H. Park, O. Simeone, and S. S. Shitz, "Optimizing Over-the-Air Computation in IRS-Aided C-RAN Systems," in *2020 IEEE 21st International Workshop on Signal Processing Advances in Wireless Communications (SPAWC)*, 2020, pp. 1–5, iSSN: 1948-3252.
- [20] H. Yang, T. Ding, and X. Yuan, "Federated learning with lossy distributed source coding: Analysis and optimization," *arXiv preprint arXiv:2204.10985*, 2022.
- [21] J. P. Vila and P. Schniter, "Expectation-maximization Gaussian-mixture approximate message passing," *IEEE Trans. Signal Process.*, vol. 61, no. 19, pp. 4658–4672, 2013.
- [22] M. P. Friedlander and M. Schmidt, "Hybrid deterministic-stochastic methods for data fitting," *Siam J. Sci. Comput.*, vol. 34, no. 3, pp. A1380–A1405, 2012.
- [23] S. Diamond and S. Boyd, "CVXPY: A python-embedded modeling language for convex optimization," *J. Mach. Learn. Res.*, vol. 17, no. 83, pp. 1–5, 2016.
- [24] F. Seide, H. Fu, J. Droppo, G. Li, and D. Yu, "1-bit stochastic gradient descent and its application to data-parallel distributed training of speech DNNs," in *Proc. Annu. Conf. Int. Speech. Commun. Assoc.*, Singapore, Singapore, 2014, pp. 1058–1062.
- [25] L. Yann, C. Corinna, and B. Christopher, "The MNIST database of handwritten digits," 1998. [Online]. Available: <http://yann.lecun.com/exdb/mnist/>
- [26] H. Xiao, K. Rasul, and R. Vollgraf, "Fashion-MNIST: A novel image dataset for benchmarking machine learning algorithms," *arXiv preprint arXiv:1708.07747*, 2017.
- [27] A. Goldsmith, *Wireless communications*. Cambridge Univer. Press, 2005.
- [28] Q. Wu and R. Zhang, "Intelligent Reflecting Surface Enhanced Wireless Network via Joint Active and Passive Beamforming," *IEEE Trans. Wirel. Commun.*, vol. 18, no. 11, pp. 5394–5409, 2019.